Neutron diffraction study of superconducting $La_3Ni_2{}^{11}B_2N_{3-\delta}$

Tahir Ali[a,b], Soner Steiner[a], Clemens Ritter[c], Herwig Michor[a,]

[a] *Institute of Solid State Physics, TU Wien, Wiedner Hauptstrasse 8–10, A-1040 Wien, Austria*
[b] *Physics Division, PINSTECH, Nilore, Islamabad, Pakistan*
[c] *Institut Laue-Langevin, B.P. 156, F-38042, Grenoble Cedex 9, France*

Abstract

We have studied structural properties of $La_3Ni_2B_2N_{3-\delta}$ samples with distinctly different values of the superconducting transition temperature by means of powder neutron diffractometry and specific heat measurements. The refinement of lattice site occupations reveals full occupations for all sites in the $La_3Ni_2{}^{11}B_2N_3$ structure with space group $I4/mmm$ except for nitrogen site N(2). For samples with T_c = 13.0 K and 13.7 K we obtain for the N(2) site distinctly different occupation factors of 0.90 and 0.93, respectively. The latter confirms a direct relation between the nitrogen stoichiometry and the superconducting transition temperature. Based on the analysis temperature dependent lattice parameters, atomic displacement factors, lattice heat capacity data and *ab initio* phonon density of states calculations we discuss the thermal expansion and vibrational properties of superconducting $La_3Ni_2B_2N_{3-\delta}$.

Keywords: superconducting materials, rare earth compounds, crystal structure, thermodynamic properties, $La_3Ni_2B_2N_{3-\delta}$

1. Introduction

A large variety of ternary and quaternary intermetallic superconductors with tetragonal crystal structures share PbO-type layers as their common structure building element (see e.g. Ref. [1]). Most prominent among them are FeAs and Fe(Se,Te) high-T_c materials [2, 3, 4], quaternary rare earth nickel borocarbide [5, 6] and boronitride superconductors [7, 8, 9], and heavy Fermion superconductors such as $CeCu_2Si_2$ [10].

It seems rather typical for members of this large family of compounds with PbO-type layers that superconducting as well as some normal state properties are rather sensitive to preparation and annealing conditions (see e.g. Refs. [11, 12] among others). In most of these cases a finite (though usually small) width of formation is responsible for a variability of the properties of certain compounds. In some cases distinct deviations of the "real structure" as compared to the idealized structure model have been reported. One example is $YNi_2{}^{10}B_2C$ where an interchange of up to 13% of boron and carbon atoms has been resolved via hot neutron diffraction [13]. A variable degree of interchange of boron and carbon possibly relates to the variability of physical properties resulting from different heat treatments of these samples and may explain the large spread of thermodynamic mean T_c-values of YNi_2B_2C ranging from about 14.2 K to 15.6 K [14, 15]. An even stronger variation of T_c from 11.7 K to 14.6 K has been reported for the boronitride superconductor $La_3Ni_2B_2N_{3-\delta}$ [16, 17, 18]. This large variation of T_c correlates inversely with the correspondent values of the residual resistivity of these samples ρ_0 varying from about 30 $\mu\Omega$cm to values down to 12 $\mu\Omega$cm [17]. We, thus, concluded that the variation of these sample dependent properties relates to a variation of the nitrogen vacancy density and accordingly to a finite width of formation with respect to the nitrogen stoichiometry in the formula $La_3Ni_2B_2N_{3-\delta}$. From a linear extrapolation of T_c versus corresponding ρ_0 data we further proposed a clean limit $T_c^{cl} \sim 16$ K for vacancy- and impurity free $La_3Ni_2B_2N_3$ which would match the T_c value reported for $LuNi_2B_2C$ [6]. A determination of the nitrogen stoichiometries by a proper technique such as neutron diffractometry was, however, still pending in our earlier report.

In this paper we present more detailed studies of $La_3Ni_2B_2N_{3-\delta}$ samples with distinctly different values of T_c = 13.0 K and 13.7 K by means of powder neutron diffractometry (PND), including studies of thermal expansion and vibrational properties. The latter are further analyzed on basis of *ab initio* phonon density of states calculations which supplements a recent theoretical study [19].

2. Material and methods

Polycrystalline samples $La_3Ni_2{}^{11}B_2N_{3-\delta}$, each with a mass of about 8 g, were prepared by inductive levitation melting employing the procedure described in the following. The starting materials are La ingot (Metall Rare Earth, 99.9%), Ni (Alpha Aesar, 99.99%), highly isotope enriched ^{11}B (Eagle Picher, chemical purity 99.9999% and isotope purity 99.97%), and nitrogen gas (Linde, 99.999 % additionally purified using an OXISORB device). In the first preparation step, stoichiomet-

**Corresponding author
Email address: michor@ifp.tuwien.ac.at (Herwig Michor)

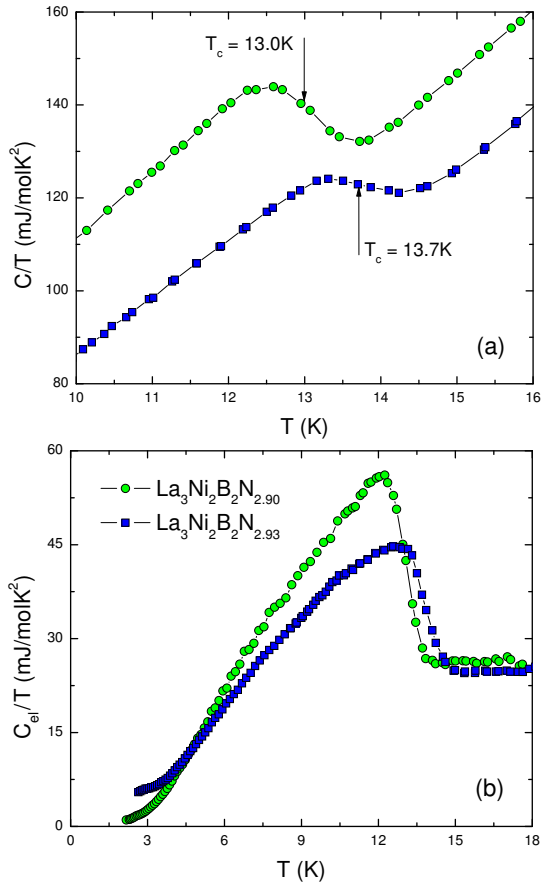

Figure 1: Temperature dependent specific heat, as C/T vs. T, of two $La_3Ni_2{}^{11}B_2N_{3-\delta}$ samples used for NPD in the upper pannel (a), where for clarity, one set of data (circles) are shifted by an offset of 15 mJ/K^{2}mol. The corresponding electronic specific heat contributions, C_{el}/T vs. T, are displayed in the lower pannel (b) with composition labels as refined from PND in section 4.1.

ric amounts of Ni and B were melted several times in Ar atmosphere to produce the binary compound NiB. In the next step, La metal was pre-melted in vacuum and then melted with NiB to prepare a $La_3Ni_2B_2$ precursor alloy. In a third step these alloys were repeatedly melted in Ar/N_2 atmosphere such that the N-stoichiometry is slowly increased to reach projected stoichiometries near $La_3Ni_2B_2N_{2.7}$ for one set of samples and projected stoichiometries near $La_3Ni_2B_2N_{2.9}$ for a second set of samples. This choice of projected stoichiometries was motivated by our earlier estimate of the width of formation of $La_3Ni_2B_2N_{3-\delta}$ [17]. The initial estimate for the nominal N-stoichiometry of each sample was obtained via measureing the mass gain after each melting cycle and by measuring the pressure drop within the recipient. As cast samples were initially heat treated in a high-vacuum furnace at 1100°C for 1 week. For a second and final annealing, samples projected as $La_3Ni_2B_2N_{\sim 2.7}$ were sealed in quartz ampoules under 200 mbar argon atmosphere and then annealed at 1130 °C for 42 hours and, finally, rapidly quenched in water. For samples with compositions projected as $La_3Ni_2B_2N_{\sim 2.9}$ the analogous final annealing procedure was applied at 1150 °C.

A first sample characterization was based on powder X-ray diffraction (XRD) using a Siemens D5000 diffractometer equipped with a graphite mono-chromator and on various low temperature techniques such as specific heat, resistivity and magnetic susceptibility measurements as described in detail earlier [20]. The characterization of the superconducting state properties of ^{11}B isotope enriched samples essentially reproduces the features discussed in Ref. [17]. Thus, for refining the positions of light elements and to measure the N-site occupancies in $La_3Ni_2{}^{11}B_2N_{3-\delta}$, neutron powder diffraction (NPD) data were collected for $La_3Ni_2{}^{11}B_2N_{3-\delta}$ samples with superconducting transition temperatures T_c = 13.0 K and T_c = 13.7 K as demonstrated by the total heat capacity data displayed in Fig. 1a and the corresponding electronic specific heat contributions displayed in Fig. 1b which have been evaluated by subtracting the lattice contributions, i.e. via normal state heat capacity data measured with an external field of 9 T (not shown). The given values of T_c are thermodynamic mean values determined by idealizing the superconducting specific heat anomalies under the constraint of entropy balance between the measured and idealized transition (see e.g. Ref. [16]). Each powder sample of 6 g was filled in a vanadium tube sample holder with a diameter of 1 cm and measured on the high resolution powder diffractometer D1A at the Institute Laue-Langevin (Grenoble, France) using a wavelength of 1.3894 Å and a 2θ range $8° < 2\theta < 159.5°$ with 0.05° or 0.1° steps. The data was collected at five different temperatures ranging from 4 K to 300 K. Full profile Rietveld refinements were carried out using the FULLPROF program [21].

3. Computational methods

The present calculations are based on the density functional theory (DFT) implemented in the Vienna *ab initio* simulation package VASP [22, 23] using a plane-wave basis and the projector-augmented wave (PAW) approach [24] for describing the electron-ion interaction. For the exchange potential the PAW local density approximation (LDA) as parametrized by Ceperley and Alder [25] was chosen. For the valence state configurations of the pseudopotentials we used $5s^25p^65d^15s^2$ states for La, $3d^93s^1$ states for Ni, $2s^2p^1$ states for B and $2s^2p^3$ states for N respectively, the remaining electrons were kept frozen.

The aim in the present *ab initio* modelling was to investigate the effect of N vacancies on the lattice properties. Accordingly, we initially performed a full relaxation of the lattice parameters and ionic positions for an 80 atom supercell with no vacancies, i.e. for a 2×2×2 supercell. The effect of vacancies is then simulated by running the calculations for a 79 atom supercell, where one N(2) atom (out of eight N(2) positions) is removed from a central point of the supercell. We again tried to fully relax the lattice parameters and ionic positions, which worked well for the vacancy free case, $La_3Ni_2B_2N_3$ (80 atoms supercell), but failed for the 79 atoms supercell. The calculations only converged for both cases, with and without vacancies, by relaxing the structure with a fixed cell shape and volume. Thereby, we have used the experimental unit cell shape and volume given by a = 0.372 nm and c = 2.052 nm. The rounding difference as compared to the exact lattice constants of both samples given in

Table 1 is not relevant with respect to the computational precision.

During the relaxation procedure, the total energy was minimized until the energy convergence became less than 1×10^{-6} eV. The size of the basis set of plane waves was defined by an energy cutoff of 500 eV. To obtain the equilibrium positions of the ions the residual forces were optimized until they became less than 1×10^{-2} eV/Å .

As a next step, the vibrational forces were calculated using the finite difference method implemented in VASP to determine the Hessian matrix, which is a linear response approach based on the DFT perturbation theory [26]. To derive the force constants, atomic displacements of 0.015 Å were chosen. Thereby, only symmetry inequivalent displacements were applied and the energy cutoff was increased to 650 eV and the total energy was minimized until the energy convergence became better than 1×10^{-8} eV. The same supercells were used for the calculations of the vibrational forces. With these forces the phonon calculations were performed by using the package `PHONOPY` [27].

The Brillouin zone integration for the relaxation of the supercells and for the calculations of the forces were done on a 3×3×2 grid of **k**-points which corresponds to a 24×24×16 grid in the Brillouin zone. For the **k**-points we have used a Monkhorst and Pack [28] mesh using the Method of Methfessel-Paxton [29], which resulted in well-converged total energies and optimized ionic positions.

4. Results and Discussion

4.1. Powder neutron diffractometry

Room temperature PND data of two samples $La_3Ni_2{}^{11}B_2N_{3-\delta}$ with distinctly different superconducting transition temperatures (see Fig. 1) are displayed in Fig. 2a (T_c = 13.0 K) and 2b (T_c = 13.7 K). Both patterns are successfully refined on the basis of the structure models of two phases [30], $La_3Ni_2B_2N_3$ (space group $I4/mmm$) and LaNiBN (space group $P4/nmm$) with practically no residual intensities (see the difference lines in Fig. 2 which corresponds to less than 1% of the total intensity). The quality of Rietveld refinements are indicated by their reliability factors, the profile factor R_p and the weighted profile factor R_{wp}, and by the goodness parameter of the fit, χ^2, as labeled in Fig. 2 (see Ref. [31] for detailed definitions). While the preceding sample characterization via powder XRD revealed essentially single phase $La_3Ni_2B_2N_3$-type patterns with almost negligible reflections from LaNiBN impurities (the two-layer variant of the quaternary boronitride), the full profile refinement of the PND pattern of two N-richer samples with $T_c \simeq 13.7$ reveals phase fractions of 19% LaNiBN for the pattern shown in Fig. 2b and 15% for the pattern of a second sample with similar nominal composition (not shown). The fraction of 19% LaNiBN-phase in the sample with $T_c \simeq 13.7$ is responsible for the markedly reduced magnitude of the superconducting specific heat anomaly as compared to the sample with T_c = 13.0 K and further responsible for the residual normal state electronic contribution of the former (see Fig. 1b).

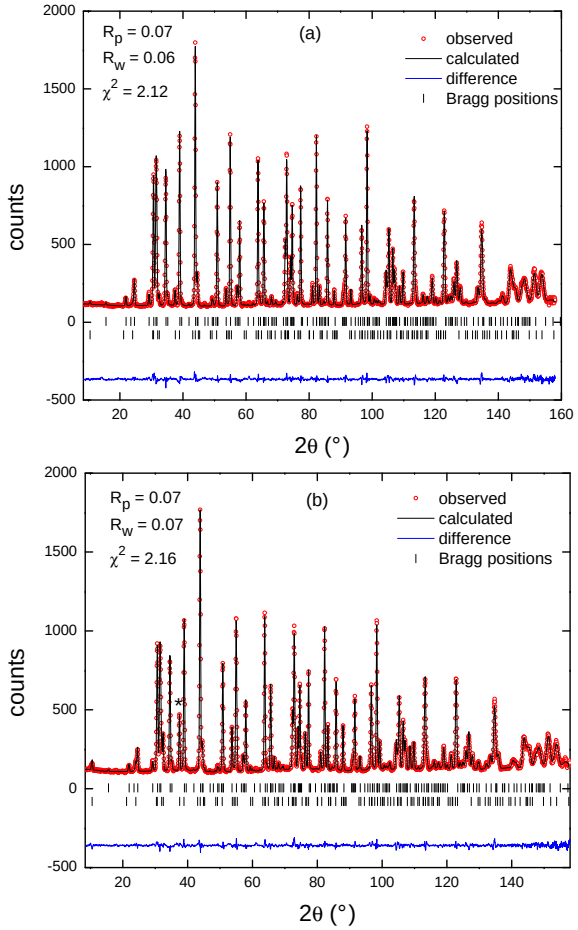

Figure 2: Measured at room temperature, calculated and difference neutron powder diffraction pattern of $La_3Ni_2{}^{11}B_2N_{3-\delta}$ with T_c = 13.0 K in the upper pannel (a) and with T_c = 13.7 K in the lower pannel (b). The upper and lower vertical bars indicate Bragg positions for $La_3Ni_2B_2N_3$ (space group $I4/mmm$) and LaNiBN (space group $P4/nmm$), respectively. The asterisk indicates the most prominent reflection of the LaNiBN impurity phase.

Observed discrepancy between our initial phase analysis based on XRD and the PND data shown in Fig. 2 obviously results from the large difference in sample volumes probed by these two methods which relates to powder masses ∼ 50 mg for XRD versus 6 g for PND. Accordingly, we subsequently collected a larger number of XRD patterns for various pieces of already available samples $La_3Ni_2B_2N_{3-\delta}$ [17] to re-evaluate our XRD based estimates of phase fractions. Thereby, some convergence with the PND results has been obtained. For $La_3Ni_2B_2N_{3-\delta}$ samples with T_c-values ranging from 12.7 K to 13.1 K essentially single XRD pattern are indeed reproducible (indicating LaNiBN fractions of less than 5%), while for T_c-values exceeding 13.1 K, LaNiBN fractions refined from individual pattern of these samples show an increasing tendency to scatter to LaNiBN phase fractions of up to about 20% (for $T_c > 13.5$ K), thus, revealing a clear trend of growing fractions of LaNiBN impurity phases for samples with highest T_c-values. Accordingly, one has to expect discrepancies between the projected stoichiometries which were evaluated in course of the

sample preparation (see section 2) and the intrinsic stoichiometry of the matrix phase $La_3Ni_2B_2N_{3-\delta}$.

The room temperature PND pattern shown in Fig. 2 as well as additional powder pattern collected at 180 K, 80 K, 30 K, and 4 K were used for analyzing the occupation factors. In the course of our initial refinements we tested the significance of refining the occupations of individual lattice sites by comparing the results obtained with all available patterns taken at different temperatures. Except for the nitrogen sites N(2) at Wyckoff position 2*b*, which is a center of inversion symmetry in the $La_3Ni_2B_2N_3$ structure, we could not achieve any sustained improvement of the refinements as compared to fixing the occupations of individual sites to one. The same conclusion was reported from an earlier PND study by Huang *et al.* [32] and is also corroborated by the results of a nuclear magnetic resonance study of ^{11}B and ^{139}La spin echo spectra [33]. Because of the close correlation between the occupation factor and the corresponding thermal parameter (B_{iso}) of each site in the structure model, the final refinements were performed with occupation factors being fixed to one, except for N(2) in $La_3Ni_2B_2N_3$, while refining the corresponding temperature dependent B_{iso} values.

The data in Table 1 summarizes the results of the Rietveld refinements indicated by the full lines in Fig. 2. The PND refinement reveals for the sample with T_c = 13.0 K in Fig. 2a a significant discrepancy between the initially projected composition $La_3Ni_2{}^{11}B_2N_{\sim 2.7}$ and the refined composition which is $La_3Ni_2{}^{11}B_2N_{2.90}$ according to the N(2) site occupation factor of 0.90. The latter is consistent with the refinements of PND data collected at five different temperatures, thus, suggesting an error bar of the occupation factor of not more than 0.005. The refinement for the sample with T_c = 13.7 K in Fig. 2b yields an N(2) site occupation factor of 0.93, thus, revealing an intrinsic composition of the matrix phase $La_3Ni_2B_2N_{2.93}$. Accordingly, there is a small but nonetheless significant difference of N(2) site occupation factor for two $La_3Ni_2{}^{11}B_2N_3$-type samples with T_c = 13.0 K and 13.7 K, respectively. For samples $La_3Ni_2B_2N_x$ with T_c values ranging from about 12 K to slightly above 14 K (see Ref. [17]) one may extrapolate on basis of the above PND results a width of formation with respect to the N-stoichiometry x ranging from $La_3Ni_2B_2N_{\sim 2.89}$ to $La_3Ni_2B_2N_{\sim 2.93}$. The corresponding N(2)-vacancy densities are thereby in approximate correspondence with the residual resistivity values ρ_0 of these samples (compare ρ_0 values reported earlier [17]). The present NPD study indicates a much narrower width of formation of $La_3Ni_2B_2N_{3-\delta}$ than proposed in Ref. [17] where nitrogen stoichiometries have been evaluated just in course of the initial sample preparation via mass gain and pressure drop when inductively melting $La_3Ni_2B_2N_x$ in Ar/N_2 atmosphere (see section 2).

4.2. Lattice parameters and lattice volume

Neutron powder diffraction performed at temperatures ranging from 4 K to 300 K allows to evaluate the thermal expansion and vibrational properties of $La_3Ni_2B_2N_{3-\delta}$. The temperature dependent variation of lattice parameters a and c of the sample with highest phase purity with a refined composition

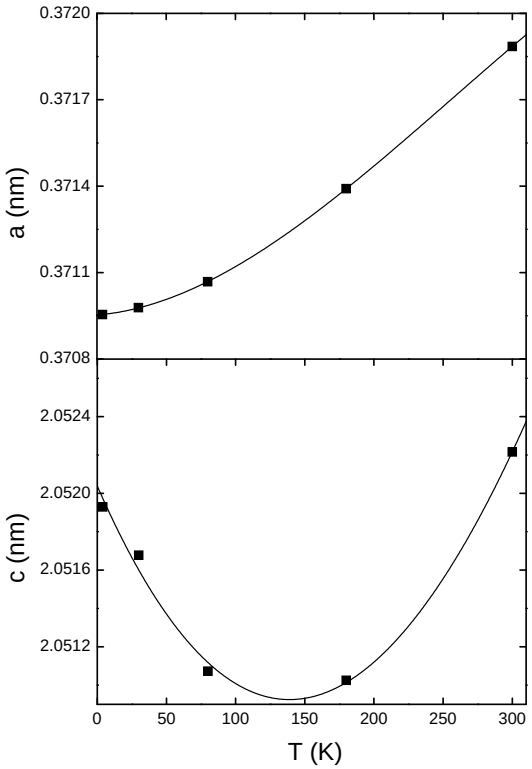

Figure 3: Temperature dependent variation of the lattice parameters a and c of $La_3Ni_2B_2N_{2.90}$; solid lines are guides to eye.

$La_3Ni_2{}^{11}B_2N_{2.90}$ (T_c = 13.0 K) is shown in Fig. 3. The temperature dependent lattice parameters reveal an expansion of the a lattice parameter with increasing temperature while the c lattice parameter shows a non-monotonic variation with a minimum around about 110 – 150 K. A similar temperature dependent variation of lattice parameters of $CeNi_2B_2C$ borocarbide [34] has been reported earlier and was explained on the basis of geometrical effects of rather rigid B-C and Ni-B bond lengths. For $La_3Ni_2B_2N_{3-\delta}$, temperature reduction causes a reduction of the volume of the La-N triple layers which is reflected by decrease in La(2)-N(2) and La(2)-N(1) distances from 0.2629 nm and 0.2542 nm at 300 K to 0.2623 nm and 0.2536 nm, respectively, at 4 K. The La(2)-N(2) distance is directly related to the a lattice parameter displayed in Fig. 3. The change in the c lattice parameter is attributed to rather rigid Ni-B bonds in the Ni_2B_2 layers. The Ni-B bond length hardly exhibits any variation with temperature. For $La_3Ni_2B_2N_{2.90}$ the Ni_2B_2 layer thickness increases from 0.2285 nm at 300 K to 0.2292 nm at 4 K. A similar increase of the Ni_2B_2 layer thickness and corresponding increase in the B-Ni-B tetrahedral angle is observed for $La_3Ni_2B_2N_{2.93}$. The second factor effecting the c lattice parameter is the thickness variation of the La-N triple layers. For $La_3Ni_2B_2N_{2.90}$ the thickness of the La-N triple layer decreases from 0.532 nm at 300 K to 0.530 nm at 80 K while it remains almost constant at further lowering of the temperature to 4 K. The non-monotonic variation of the c lattice parameter, thus, results from the addition of positive and negative contributions to

$La_3Ni_2{}^{11}B_2N_{3-\delta}$ with T_c = 13.0 K						
a = 0.37188(2) nm, c = 2.05222(2) nm, V = 0.28382(1)nm^3, c/a = 5.5185						
Atom	Site	x	y	z	B_{iso}	Occ.
La(2)	2a	0.0000	0.0000	0.00000	0.430(12)	1.00
La(1)	4e	0.0000	0.0000	0.37037(4)	0.413(12)	1.00
Ni	4d	0.0000	0.5000	0.25000	0.551(11)	1.00
B	4e	0.0000	0.0000	0.19433(6)	0.761(17)	1.00
N(1)	4e	0.0000	0.0000	0.12390(4)	0.611(13)	1.00
N(2)	2b	0.0000	0.0000	0.50000	0.655(13)	0.90
$La_3Ni_2{}^{11}B_2N_{3-\delta}$ with T_c = 13.7 K						
a = 0.37181(2) nm, c = 2.05252(2) nm, V = 0.28375(1)nm^3, c/a = 5.5203						
Atom	Site	x	y	z	B_{iso}	Occ.
La(2)	2a	0.0000	0.0000	0.00000	0.414(15)	1.00
La(1)	4e	0.0000	0.0000	0.37075(5)	0.398(15)	1.00
Ni	4d	0.0000	0.5000	0.25000	0.573(13)	1.00
B	4e	0.0000	0.0000	0.19413(7)	0.786(21)	1.00
N(1)	4e	0.0000	0.0000	0.12397(5)	0.602(16)	1.00
N(2)	2b	0.0000	0.0000	0.50000	0.648(16)	0.93

Table 1: Room temperature NPD data of two samples $La_3Ni_2{}^{11}B_2N_{3-\delta}$ as labeled.

		4 K	30 K	80 K	180 K	300 K
	a (nm)	0.37095(2)	0.37097(2)	0.37106(2)	0.37139(2)	0.37188(2)
	c (nm)	2.05193(2)	2.05168(2)	2.05107(2)	2.05102(2)	2.05222(2)
	c/a	5.530	5.531	5.528	5.522	5.5185
	V (nm^3)	0.28236(1)	0.28236(1)	0.28241(1)	0.28290(1)	0.28382(1)
	z(La1)	0.37068(7)	0.37071(7)	0.37074(7)	0.37057(7)	0.37037(4)
	z(N1)	0.12360(7)	0.12358(7)	0.12368(7)	0.12369(7)	0.12390(4)
	z(B)	0.19414(9)	0.19415(9)	0.19411(9)	0.19422(8)	0.19433(6)
B_{iso} (Å^2)	La(2)	0.144(18)	0.159(18)	0.174(17)	0.259(17)	0.430(12)
	La(1)	0.127(18)	0.142(18)	0.157(17)	0.242(17)	0.413(12)
	Ni	0.223(17)	0.227(16)	0.272(16)	0.386(16)	0.551(11)
	B	0.396(28)	0.414(26)	0.440(26)	0.545(25)	0.761(17)
	N(1)	0.353(20)	0.350(19)	0.390(19)	0.477(19)	0.611(13)
	N(2)	0.398(20)	0.396(19)	0.436(19)	0.492(19)	0.655(13)
R-factors	R_p (%)	7.70	7.23	7.25	7.04	6.93
	R_{wp} (%)	7.54	7.12	7.04	6.77	6.54
	χ^2	2.96	2.91	2.80	2.44	2.12

Table 2: Crystal structure and lattice parameter data for $La_3Ni_2B_2N_{2.90}$ at various temperatures as listed.

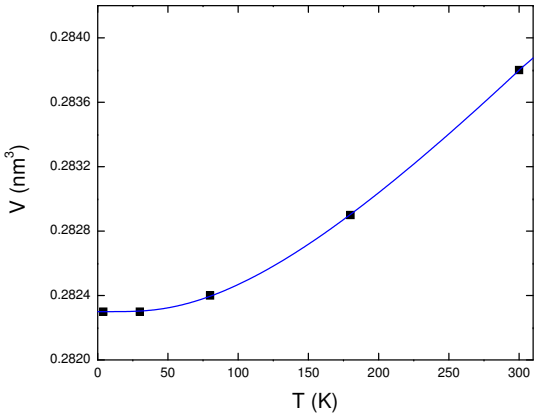

Figure 4: Temperature dependent unit cell volume of $La_3Ni_2B_2N_{2.90}$; the solid line indicates a fit of these volume thermal expansion data by equations 1 and 2 (see text).

the c-axis expansion from Ni_2B_2 and La-N triple layers. When cooling from room temperature down to 150 K, the reduction in the La-N triple layer thickness dominates over the increase in the Ni_2B_2 layer thickness resulting in a decrease in the c lattice parameter. At temperatures below 100 K the thickness of the La-N triple layers becomes almost constant, thus, resulting in an increase in the c lattice parameter due to the further increase in the B-Ni-B tetrahedral angle.

The temperature dependent variation of the unit-cell volume of $La_3Ni_2B_2N_{2.90}$ is shown in Fig. 4. The solid line displays a fit based on the Grüneisen approximation for the zero-pressure equation of state, by which the effects of the thermal expansion are considered to be equal to the elastic strain [35]. To first order the temperature dependence of the volume can be described by

$$V(T) = \frac{\gamma U(T)}{K_o} + V_o \qquad (1)$$

where γ is the Grüneisen parameter, K_o is the bulk modulus, V_o is the volume at $T = 0$ K. The internal energy, $U(T)$, due to phonon contributions is given by

$$U(T) = \int \frac{\hbar\omega F(\omega)}{e^{\frac{\hbar\omega}{k_B T}} - 1} d\omega, \qquad (2)$$

where $F(\omega)$ is the phonon density of states which has been calculated for $La_3Ni_2B_2N_{2.875}$ from *ab initio* (see next section 4.3). The temperature dependent variation of the lattice volume is well described by the above model as demonstrated by the solid line in Fig. 4. The fit yields $\gamma/K_o = 1.22 \times 10^{-11}$ Pa^{-1} and $V_o = 0.2823$ nm^3. We note, that a fit of $V(T)$ by using equation 1 with a simple Debye approximation of the internal energy gives a clearly less perfect description of the experimental data as compared to the present approach based on a detailed model of $F(\omega)$ in equation 2.

4.3. Vibrational properties

The vibrational properties of $La_3Ni_2B_2N_{2.90}$ were investigated by means of specific heat measurements and by analyzing the temperature dependent atomic displacement parameters

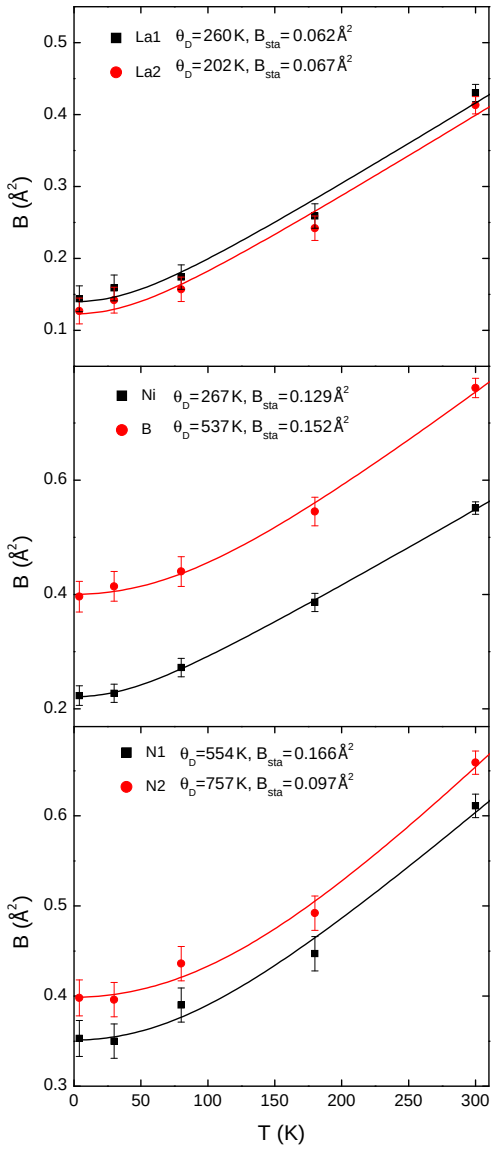

Figure 5: Temperature dependent isotropic thermal parameters of different lattice sites in $La_3Ni_2B_2N_{2.90}$. Solid lines are fits according to equation 3 and the resulting Debye temperatures Θ_D and B_{sta} of each site are given in the labels.

(ADP) obtained from the PND refinements. The latter, i.e. B_{iso} of each lattice site, are shown for $La_3Ni_2B_2N_{2.90}$ ($T_c = 13.0$ K) in Fig. 5. The isotropic ADP are related to the mean-square displacement amplitudes $< U_{iso} >$ of the corresponding lattice sites as [36]

$$B_{iso} = 8\pi\langle U_{iso}^2\rangle + B_{sta} \qquad (3)$$

where B_{sta} is the component of the thermal parameter caused by the presence of static disorder in the lattice. Within the Debye model the $U_{iso}(T)$ is given as [37]

$$< U_{iso}^2 >= \frac{3h^2T}{4\pi^2 m k_B \Theta_D^2}\left[\frac{T}{\Theta_D}\int_0^{\frac{\Theta_D}{T}} \frac{x}{e^x - 1}dx + \frac{\Theta_D}{4T}\right] \qquad (4)$$

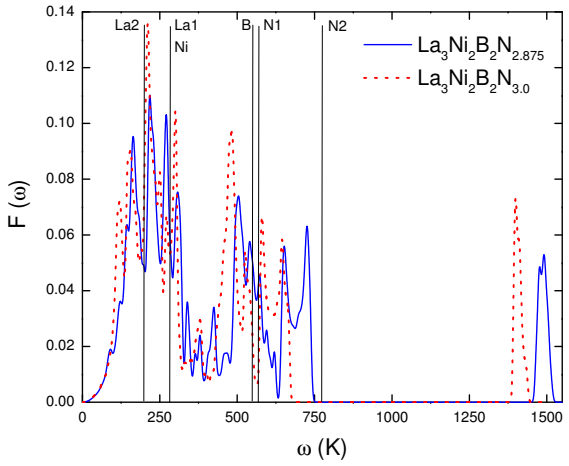

Figure 6: Calculated phonon density of states, $F(\omega)$, of $La_3Ni_2B_2N_{3.0}$ (dashed line) and $F(\omega)$ obtained wit a $La_3Ni_2B_2N_{2.875}$ supercell calculation (solid line). Vertical lines indicate Debye frequencies of individual lattice sites evaluated from temperature dependent isotropic thermal ADP (see Fig. 5).

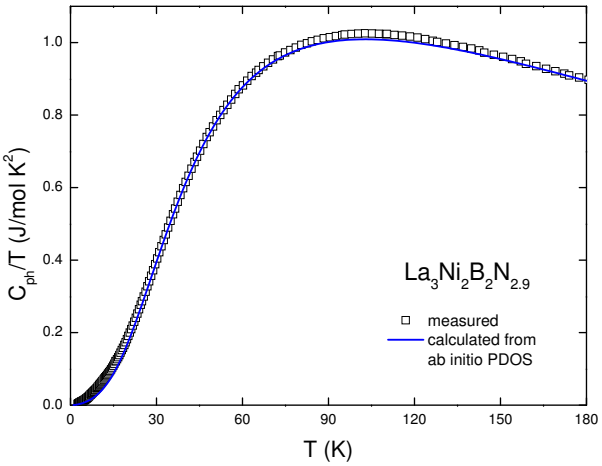

Figure 7: Temperature dependent lattice heat capacity of $La_3Ni_2B_2N_{2.90}$. The solid line represents the heat capacity calculated from the DFT phonon spectrum of the $La_3Ni_2B_2N_{2.875}$ supercell on the basis of equation 5.

with Θ_D being a characteristic Debye temperature related to the vibrational behavior of atoms at a specific crystallographic site. At lowest temperatures U_{iso} reaches the zero point value of $3h^2/16\pi^2 m k_B \Theta_D$. The temperature dependent ADP of all crystallographic sites for sample $La_3Ni_2B_2N_{2.90}$ are analyzed on the basis of equations (3) and (4) and the corresponding fits are displayed as solid lines in Fig. 5. The Debye temperatures are summarized in labels of Fig. 5 and indicated in Fig. 6. The Debye frequencies of La and Ni indicate a similar range of phonon frequencies for their respective lattice sites. The Debye frequencies of B and N(1) are also comparable, while that of N(2) located in central LaN layer displays the highest characteristic frequency.

For an in-depth analysis of vibrational properties of $La_3Ni_2B_2N_{3-\delta}$ we performed DFT calculations of inter-atomic forces in order to derive a model for the phonon dispersions (see section 3). The resulting phonon density of states (PDOS) obtained from DFT calculations is shown in Fig. 6. The PDOS of vacancy free $La_3Ni_2B_2N_3$ is displayed as dashed line and that of a supercell calculation where one out of eight N(2) positions is left vacant, i.e. for $La_3Ni_2B_2N_{2.875}$, is shown as a solid line in Fig. 6. The former essentially reproduces recent PDOS results of $La_3Ni_2B_2N_3$ reported by Tütüncü *et al.* [19]. The slightly more realistic supercell calculation with vacancies, however, shifts spectral weight towards higher energies which in fact significantly improves the agreement with the experimental evaluation of the lattice heat capacity of $La_3Ni_2B_2N_{2.9}$. The lattice heat capacity relates to $F(\omega)$ via

$$C_{ph}(T) = R \int F(\omega) \frac{\left(\frac{\omega}{2T}\right)^2}{\sinh^2\left(\frac{\omega}{2T}\right)} d\omega, \qquad (5)$$

where $F(\omega)$ is the phonon spectrum obtained from *ab initio* calculations. Via Eqn. 5, $C_{ph}(T)$ is evaluated for the $La_3Ni_2B_2N_{2.875}$ supercell calculation and compared in Fig. 7 with the lattice heat capacity obtained from experimental data where the electronic contribution has been subtracted from the measured total heat capacity of $La_3Ni_2B_2N_{2.90}$. The calculated $C_{ph}(T)$ is indicated as a solid line in Fig. 7 revealing close agreement with the experimental result. We emphasize, that the shift of spectral weights in the calculation for $La_3Ni_2B_2N_{2.875}$ as compared to that of vacancy free $La_3Ni_2B_2N_3$ is due to the relaxation of atomic positions and charge distribution in the vicinity of the vacancies and not related to a volume effect which has been suppressed in the computational setup (see section 3).

The present *ab initio* modeling of the PDOS of $La_3Ni_2B_2N_{2.90}$ shows that an earlier attempt of fitting the PDOS purely on the base of specific heat data in Ref. [14] suits to describe the low energy part of the PDOS, but clearly fails with respect to any details of the PDOS at higher energies. However, with respect to a rough characterization of the PDOS, $F(\omega)$, in terms of its generalized moments, $\omega_{\ln}$, $\overline{\omega}_1$, and $\overline{\omega}_2$, as defined by Allen and Dynes [38] the earlier results are rather well confirmed. The re-evaluation of these moments using the calculated PDOS data of $La_3Ni_2B_2N_{2.875}$ in Fig. 6 (solid blue line) yields $\omega_{\ln} = 227\,\mathrm{K}$, $\overline{\omega}_1 = 283\,\mathrm{K}$ and $\overline{\omega}_2 = 356\,\mathrm{K}$ in fair agreement with $\omega_{\ln} = 218\,\mathrm{K}$, $\overline{\omega}_1 = 273\,\mathrm{K}$ and $\overline{\omega}_2 = 333\,\mathrm{K}$ reported in Ref. [14].

To compare the experimental estimates of local atomic modes with the *ab initio* PDOS, all Debye frequencies of individual lattice sites obtained from isotropic ADP are indicated as vertical lines in Fig. 6. It is evident that the low frequency vibrational spectrum at energies corresponding up to $\sim 250\,\mathrm{K}$ is dominated by the heavy atoms La and Ni. Above energies corresponding to 400 K the dominant contribution to the phonon DOS comes from vibrations of lighter elements B and N. In contrary to borocarbide superconductors like $LuNi_2B_2C$ which display a very specific, soft optical phonon branch which crosses with acoustic branches at energies around 10 – 15 meV [39], the PDOS of $La_3Ni_2B_2N_{3-\delta}$ origins in the low energy range up to about 20 meV essentially from transverse and longitudinal acoustic branches. For detailed discussions of the

phonon dispersions we refer to Ref. [19].

Hydrostatic pressure electrical resistivity studies of $La_3Ni_2B_2N_{3-\delta}$ revealed close interrelations between the effects of the applied pressure upon the superconducting transition temperature, $T_c(p)$, the Debye temperature, $\Theta_D(p)$, and the residual resistivity, $\rho_0(p)$ [16, 17]. Thereby, a reduction of T_c relates to a pressure induced lattice stiffening (increase of Θ_D) and in addition to pressure enhanced potential scattering (increase of ρ_0). Though these two reports revealed markedly different initial pressure dependencies $dT_c/dp \simeq -130$ mK/kbar for $La_3Ni_2B_2N_{3-\delta}$ with $T_c^\rho \simeq 12.3$ K [16] and $dT_c/dp \simeq -80$ mK/kbar for $La_3Ni_2B_2N_{\sim 2.92}$ with $T_c^\rho \simeq 14.6$ K [17], very similar relations between dT_c/dp, $d\rho_0/dp$, and $d\Theta_D/dp$ have been observed. We, thus, expect that the lattice stiffening due to the precence of nitrogen vacancies indicated by the *ab initio* PDOS results in Fig. 6 is co-reponsible for the significant variation of T_c in $La_3Ni_2B_2N_{3-\delta}$ discussed in Ref. [17]. A second factor is, of course, Cooper pair breaking due to defect scattering which, however, in the present case of *s*-wave superconductivity is expected to be a minor effect on T_c.

4.4. Summary and Conclusions

Powder neutron diffraction measurements on $La_3Ni_2{}^{11}B_2N_{3-\delta}$ were performed at temperatures ranging from 4 K to 300 K. The Rietveld analysis of PND pattern collected for samples displaying distinctly different values of the superconducting transition temperature, $T_c = 13.0$ K and $T_c = 13.7$ K, revealed distinctly different occupation factors of the nitrogen N(2) sites with 0.90 and 0.93, respectively. These PND results, thus, indicate a much narrower width of formation with respect to the nitrogen stoichiometry than expected from our earlier study [17].

The thermal expansion behavior of $La_3Ni_2{}^{11}B_2N_{2.90}$ revealed by the temperature dependent lattice constants displays for the *a* lattice parameter a normal expansion with increasing temperature, while the *c* lattice parameter displays a non-monotonic variation with a minimum around 110 – 150 K. The latter is discussed in terms of the Ni-B bonding geometry. The temperature dependence of the volume thermal expansion as obtained from the present NPD data is, nonetheless, well in line with a first order Grüneisen approximation for the zero-pressure equation of state when using our result of the *ab initio* calculated PDOS for computing the temperature dependent internal energy of the lattice. From the analysis of temperature dependent atomic displacement factors in terms of a simple Debye model we determined characteristic vibration frequencies of individual lattice sites which compare reasonably well with the PDOS calculated for a $La_3Ni_2B_2N_{2.875}$ super cell.

The comparison of the present PDOS models for $La_3Ni_2B_2N_3$ and $La_3Ni_2B_2N_{2.875}$ with the experimentally evaluated lattice heat capacity data affirms the relevance of the N(2) vacancies to the vibrational properties of $La_3Ni_2{}^{11}B_2N_{2.90}$. Much better agreement with the experiment is obtained for a supercell calculation with vacancies.

References

[1] F. Ronning, E. Bauer, T. Park, N. Kurita, T. Klimczuk, R. Movshovich, A. Sefat, D. Mandrus, J. Thompson, Ni_2X_2 (X = pnictide, chalcogenide, or B) based superconductors, Physica C: Superconductivity 469 (2009) 396 – 403. doi:10.1016/j.physc.2009.03.031.

[2] Y. Kamihara, T. Watanabe, M. Hirano, H. Hosono, Iron-based layered superconductor La[$O_{1-x}F_x$]FeAs (x = 0.05–0.12) with T_c = 26 K, Journal of the American Chemical Society 130 (2008) 3296 – 3297. doi:10.1021/ja800073m.

[3] F.-C. Hsu, J.-Y. Luo, K.-W. Yeh, T.-K. Chen, T.-W. Huang, P. M. Wu, Y.-C. Lee, Y.-L. Huang, Y.-Y. Chu, D.-C. Yan, M.-K. Wu, Superconductivity in the PbO-type structure α-FeSe, Proc. Natl. Acad. Sci. 105 (2008) 14262 – 14264. doi:10.1073/pnas.0807325105.

[4] K.-W. Yeh, T.-W. Huang, Y. lin Huang, T.-K. Chen, F.-C. Hsu, P. M. Wu, Y.-C. Lee, Y.-Y. Chu, C.-L. Chen, J.-Y. Luo, D.-C. Yan, M.-K. Wu, Tellurium substitution effect on superconductivity of the α-phase iron selenide, Europhys. Lett. 84 (2008) 37002. doi:10.1209/0295-5075/84/37002.

[5] R. Nagarajan, C. Mazumdar, Z. Hossain, S. K. Dhar, K. V. Gopalakrishnan, L. C. Gupta, C. Godart, B. D. Padalia, R. Vijayaraghavan, Bulk superconductivity at an elevated temperature ($T_c \approx$12 K) in a nickel containing alloy system Y-Ni-B-C, Phys. Rev. Lett. 72 (1994) 274–277. doi:10.1103/PhysRevLett.72.274.

[6] R. Cava, H. Takagi, H. Zandbergen, J. Krajewski, W. Peck, T. Siegrist, B. Batlogg, R. Van Dover, R. Felder, K. Mizuhashi, et al., Superconductivity in the quaternary intermetallic compounds $LnNi_2B_2C$, Nature 367 (1994) 252–253. doi:10.1038/367252a0.

[7] R. Cava, H. Zandbergen, B. Batlogg, H. Eisaki, H. Takagi, J. Krajewski, W. Peck, E. Gyorgy, S. Uchida, Superconductivity in lanthanum nickel boro-nitride, Nature 372 (1994) 245–247. doi:10.1038/372245a0.

[8] T. Ali, E. Bauer, G. Hilscher, H. Michor, Structural, superconducting and magnetic properties of $La_{3-x}R_xNi_2B_2N_{3-\delta}$ with R = Ce, Pr, Nd, Solid State Phenomena 170 (2011) 165–169. doi:10.4028/www.scientific.net/SSP.170.165.

[9] N. Imamura, H. Mizoguchi, H. Hosono, Superconductivity in LaTMBN and $La_3TM_2B_2N_3$ (TM = transition metal) synthesized under high pressure, Journal of the American Chemical Society 134 (2012) 2516–2519. doi:10.1021/ja211293x.

[10] F. Steglich, J. Aarts, C. D. Bredl, W. Lieke, D. Meschede, W. Franz, H. Schäfer, Superconductivity in the presence of strong Pauli paramagnetism: $CeCu_2Si_2$, Phys. Rev. Lett. 43 (1979) 1892–1896. doi:10.1103/PhysRevLett.43.1892.

[11] A. Dertinger, R. E. Dinnebier, A. Kreyssig, P. W. Stephens, S. Pagola, M. Loewenhaupt, S. van Smaalen, H. F. Braun, Microscopic changes in $HoNi_2B_2C$ due to thermal treatment and its effect on superconductivity, Phys. Rev. B 63 (2001) 184518. doi:10.1103/PhysRevB.63.184518.

[12] S. Seiro, M. Deppe, H. Jeevan, U. Burkhardt, C. Geibel, Flux crystal growth of $CeCu_2Si_2$: Revealing the effect of composition, physica status solidi (b) 247 (2010) 614–616. doi:10.1002/pssb.200983039.

[13] A. Hillier, R. Smith, R. Cywinski, Evidence for boron–carbon disorder in $YNi_2^{10}B_2C$, Applied Physics A 74[Suppl.] (2002) s823–s825. doi:10.1007/s003390101154.

[14] H. Michor, T. Holubar, C. Dusek, G. Hilscher, Specific-heat analysis of rare-earth transition-metal borocarbides: An estimation of the electron-phonon coupling strength, Phys. Rev. B 52 (1995) 16165–16175. doi:10.1103/PhysRevB.52.16165.

[15] S. Manalo, H. Michor, M. El-Hagary, G. Hilscher, E. Schachinger, Superconducting properties of $Y_xLu_{1-x}Ni_2B_2C$ and $La_3Ni_2B_2N_{3-\delta}$: a comparison between experiment and Eliashberg theory, Phys. Rev. B 63 (2001) 104508. doi:10.1103/PhysRevB.63.104508.

[16] H. Michor, R. Krendelsberger, G. Hilscher, E. Bauer, C. Dusek, R. Hauser, L. Naber, D. Werner, P. Rogl, H. W. Zandbergen, Superconducting properties of $La_3Ni_2B_2N_{3-\delta}$, Phys. Rev. B 54 (1996) 9408–9420. doi:10.1103/PhysRevB.54.9408.

[17] T. Ali, C. Rupprecht, R. Khan, E. Bauer, G. Hilscher, H. Michor, The effect of nitrogen vacancies in $La_3Ni_2B_2N_{3-\delta}$, Journal of Physics: Conference Series 200 (2010) 012004. doi:10.1088/1742-6596/200/1/012004.

[18] B. Blaschkowski, H.-J. Meyer, X-ray single crystal refinement and superconductivity of $La_3Ni_2B_2N_3$, Zeitschrift für anorganische und allgemeine Chemie 629 (1) (2003) 129–132. doi:10.1002/zaac.200390004.

[19] H. M. Tütüncü, E. Karaca, G. P. Srivastava, Electron-phonon interaction and superconductivity in the $La_3Ni_2B_2N_3$, Philosophical Magazine 97 (2017) 128–143. doi:10.1080/14786435.2016.1245881.

[20] T. Ali, E. Bauer, G. Hilscher, H. Michor, Anderson lattice in the intermediate valence compound $Ce_3Ni_2B_2N_{3-\delta}$, Phys. Rev. B 83 (2011) 115131. doi:10.1103/PhysRevB.83.115131.

[21] J. Rodríquez-Carvajal, T. Roisnel, Winplotr: A windows tool for powder diffraction pattern analysis, in: R. Delhez, E. Mittemeijer (Eds.), European Powder Diffraction EPDIC 7, Vol. 378–381 of Materials Science Forum, Trans Tech Publications, 2001, pp. 118–123. doi:10.4028/www.scientific.net/MSF.378-381.118.

[22] G. Kresse, J. Furthmüller, Efficient iterative schemes for ab initio total-energy calculations using a plane-wave basis set, Phys. Rev. B 54 (1996) 11169–11186. doi:10.1103/PhysRevB.54.11169.

[23] G. Kresse, D. Joubert, From ultrasoft pseudopotentials to the projector augmented-wave method, Phys. Rev. B 59 (1999) 1758–1775. doi:10.1103/PhysRevB.59.1758.

[24] P. E. Blöchl, Projector augmented-wave method, Phys. Rev. B 50 (1994) 17953–17979. doi:10.1103/PhysRevB.50.17953.

[25] D. M. Ceperley, B. J. Alder, Ground state of the electron gas by a stochastic method, Phys. Rev. Lett. 45 (1980) 566–569. doi:10.1103/PhysRevLett.45.566.

[26] G. Kresse, J. Furthmüller, J. Hafner, Ab initio force constant approach to phonon dispersion relations of diamond and graphite, EPL (Europhysics Letters) 32 (1995) 729–734.
URL http://stacks.iop.org/0295-5075/32/i=9/a=005

[27] A. Togo, I. Tanaka, First principles phonon calculations in materials science, Scripta Materialia 108 (2015) 1–5. doi:10.1016/j.scriptamat.2015.07.021.

[28] H. J. Monkhorst, J. D. Pack, Special points for brillouin-zone integrations, Phys. Rev. B 13 (1976) 5188–5192. doi:10.1103/PhysRevB.13.5188.

[29] M. Methfessel, A. T. Paxton, High-precision sampling for brillouin-zone integration in metals, Phys. Rev. B 40 (1989) 3616–3621. doi:10.1103/PhysRevB.40.3616.

[30] H. Zandbergen, J. Jansen, R. Cava, J. Krajewskii, W. Peck, Structure of the 13 K superconductor $La_3Ni_2B_2N_3$ and the related phase LaNiBN, Nature 372 (1994) 759–761. doi:10.1038/372759a0.

[31] M. F. C. Ladd, R. A. Palmer, Structure Determination by X-ray Crystallography, Springer, New York, 2013. doi:10.1007/978-1-4614-3954-7.

[32] Q. Huang, B. Chakoumakos, A. Santoro, R. Cava, J. Krajewski, W. P. Jr., Neutron powder diffraction study of the 12 K superconductor $La_3Ni_2B_2N_{3-x}$, Physica C: Superconductivity 244 (1995) 101 – 105. doi:10.1016/0921-4534(95)00041-0.

[33] M. W. Pieper, H. Michor, T. Ali, NMR compared to band structure calculations of the quaternary superconductor $La_3Ni_2B_2N_{3-x}$, Phys. Rev. B 85 (2012) 214510. doi:10.1103/PhysRevB.85.214510.

[34] J. W. Lynn, S. Skanthakumar, Q. Huang, S. K. Sinha, Z. Hossain, L. C. Gupta, R. Nagarajan, C. Godart, Magnetic order and crystal structure in the superconducting RNi_2B_2C materials, Phys. Rev. B 55 (1997) 6584–6598. doi:10.1103/PhysRevB.55.6584.

[35] D. C. Wallace, Thermodynamics of Crystals, Courier Corporation, 1998.

[36] C. Wang, K. Girgis, Neutron diffraction determination of the Debye temperature of $TmGa_{2-x}Al_x$ alloys (x = 0, 0.5, 1.75), J. Less Comm. Met. 158 (1990) 319 – 325. doi:10.1016/0022-5088(90)90067-T.

[37] B. T. M. Willis, A. W. Pryor, Thermal Vibrations in Crystallography, Vol. 1, Cambridge University Press Cambridge, 1975.

[38] P. B. Allen, R. C. Dynes, Transition temperature of strong-coupled superconductors reanalyzed, Phys. Rev. B 12 (1975) 905–922. doi:10.1103/PhysRevB.12.905.

[39] P. Dervenagas, M. Bullock, J. Zarestky, P. Canfield, B. K. Cho, B. Harmon, A. I. Goldman, C. Stassis, Soft phonons in superconducting $LuNi_2B_2C$, Phys. Rev. B 52 (1995) R9839–R9842. doi:10.1103/PhysRevB.52.R9839.